Proceedings of the ASME 2020 15th International Manufacturing Science and Engineering Conference
MSEC2020
September 3, 2020, Virtual, Online

MSEC2020-8394

INTENSE PULSE LIGHT ANNEALING FOR PEROVSKITE PHOTOVOLTAICS

Amir H. Ghahremani, Thad Druffel[1]
University of Louisville
Louisville, KY

ABSTRACT

Rapid advancements within photovoltaics realm necessitates swift fabrication of the modules using cheap materials through cost effective manufacturing processes to achieve short cost payback time. Photovoltaics manufacturing includes chemical processing of the materials followed by thermal annealing. Yet, long-term annealing of the materials using high temperature furnaces have remained the prevalent post-processing approach in industry which necessitates alternative methods to achieve high performance modules through rapid and economical processes. Intense pulse light (IPL) has been successfully applied as a promising rapid post-process annealing for various thin film photovoltaics, particularly to process the organic-inorganic perovskite solar cell (PSC) layers. In this paper, several results pertinent to the application of IPL on perovskite and SnO_2 electron transport thin films are presented and the role of IPL on rapid thermal annealing (RTA) is explained. We show that swift fabrication of PSCs through IPL can result in efficiencies exceeding 16% when the Perovskite film is annealed with aid of CH_2I_2 alkyl halide additive in the ambient with 60% relative humidity. In addition, the synergy of IPL-alkyl halide interaction for other perovskite chemistries is introduced. We show that achieving to PSCs exceeding 12% efficiency was possible when the perovskite and SnO_2 ETL was annealed sequentially through IPL.

Keywords: Intense Pulse Light, Perovskite solar cell, Rapid Thermal Annealing.

1. INTRODUCTION

Advancements within material processing, deposition, and annealing of perovskite solar cells (PSCs) has resulted in staggering efficiency improvement of this photovoltaics exceeding 25% [1]. Enhancement within material processing has been indebted to the tremendous research and development efforts carried out to take the advantage of potential materials and techniques to alter the band gap of material, diminish the exciton binding energy, enhance the charge carrier diffusion length, and improve the optical absorption [2-5]. Similarly, various deposition techniques such as multi-step coating process, use of antisolvents, and additives have resulted in superior morphology thin films with high uniformity [6-8].

Thermal annealing is a significant factor which affects the efficiency of device modules, the manufacturing cost, and production speed; yet, PSC thin films have been annealed through high temperature furnaces, ovens, and radiative annealing for long-term. Therefore, it is important to meet the most optimum energy payback time through application of alternative means to anneal the thin film materials.

Intense pulse light (IPL) is an extremely rapid thermal annealing (RTA) approach which can crystallize and sinter the material and composites within ultrashort duration without providing sufficient time to degrade the exposing thin film and the underneath layers; thus, it can be a suitable option for economical and high speed production of PSC modules [9]. IPL enables large area thin film annealing while preserving the uniformity as well as providing instant and optimum post processing of various thin films containing organic and inorganic compounds with respect to market needs. IPL takes the advantage of a broad light spectrum from IR to UV to sinter the material and has the working principle similar to gas discharge lamps, in which, the relaxation of the excited noble gas atoms upon the application of high voltage to the lamp releases

[1] Contact author: Thad.druffel@louisville.edu

tremendous energy capable to anneal the materials. Therefore, research within pertinent realms such as flash counts, flash energy, flash dwell time, and delay between pulses is expected to deliver different degrees of material crystallinity.

Herein, we introduce several results obtained from flash annealing of the charge carrier and perovskite light absorber thin films through characterization methods. The results include the evolution of chemical state, degree of crystallization, and their impact on thin film morphology and device photovoltaic performance. The material characterization methods include morphological inspections through scanning electron microscopy (SEM), photo absorption using UV-Vis, phase purity and crystallinity through X-ray diffraction (XRD), chemical state observations through X-ray photoelectron spectroscopy (XPS), interfacial charge transportation capability through impedance spectroscopy (IS) and photoluminescence (PL), and device photovoltaic parameters through voltammetry techniques. The obtained results designate IPL as a promising RTA approach for high throughput and industrial scale manufacturing of photovoltaic modules, particularly PSCs.

2. MATERIALS AND METHODS

2.1 Materials

PbI_2 (99.9985%), N,N-Dimethylformamide (99.8%), di-iodomethane (CH_2I_2, 99%), and SnO_2 solution (15% in H_2O colloidal dispersion) were purchased from Alfa Aesar. Methylammonium iodide (MAI), Formamidinium iodide (FAI), and cobalt dopant FK209 were purchased from Greatcell solar. The 2,2,7,7-Tetrakis(N,N-di-p-methoxyphenylamine)-9,9-spirobifluorene (Spiro-MeOTAD) was acquired from Merck. FTO glass substrates (< 20 Ω/sq., 2 cm × 2 cm × 3 mm) and gold palettes (99.999%) were purchased from Hartford glass and Kurt J. Lesker Co., respectively. All other materials were purchased from Sigma Aldrich.

2.2 Device Fabrication

FTO glass slides (2 cm × 2 cm × 3 mm) were etched using zinc powder and 2M HCl and were cleaned through sequential sonication in a 1:10 V/V diluted solution of Hellmanex detergent in DI water, DI water, ethanol, and DI water for 10 min each. After blowing with nitrogen to remove the remainder water, plasma treatment was applied to the cleaned substrates for 10 minutes to improve the surface hydrophilicity. The SnO_2 ETL was then spin coated from a 1:4 V/V diluted solution of the SnO_2 colloidal dispersion in fresh DI water using the spinning rate of 2000 rpm for 30 seconds to obtain 15-40 nm film, and the electrode places were wiped off with cotton swabs dipped in DI water. The substrates were immediately transferred to an IPL machine to perform the annealing process using different flash counts having different energy quantities and were later put under a UV lamp to provide surface treatment and remove the organic contaminants for 15 minutes. The perovskite ink passed through a 0.45 µm PTFE syringe filter was then spin-coated on SnO_2 coated substrates at two consecutive spinning rates of 1000 rpm for 10 seconds and 3000 rpm for 30 seconds to form the thickness of about 300 nm. During the last 12 seconds of the spinning process, 200 µl of chlorobenzene solution was pipetted on the rotating substrate to take the solution to the supersaturation mode and form a transparent yellow wet film. The $CH_3NH_3PbI_3$ perovskite ink was made by dissolving 1.4 mole PbI_2 and 1.4 mole of CH_3NH_3I in 1 ml DMF, 0.125 DMSO in a nitrogen filled glovebox. After complete dissolution and the formation of a transparent yellow solution, 0.25 mL di-iodomethane (CH_2I_2) was pipetted to the solution and stirred until complete dissolution. The $Cs_{0.05}(MA_{0.85}FA_{0.15})_{0.95}PbI_3$ triple cation perovskite ink was made in a nitrogen filled glovebox by dissolving 0.013 gr CsI, 0.6454 gr PbI_2, 0.0343 gr FAI, and 0.18 gr MAI in the similar $CH_3NH_3PbI_3$ perovskite solvent mixture. During the spinning process, a dry air stream was put in the spin coater chamber to keep the relative humidity less than 10%. After heating the wet perovskite film for 20 seconds on a hotplate at 110°C, the slides were immediately taken to the IPL machine to perform rapid perovskite annealing through 5 pulses, each with 1.4 kJ energy. Both hotplate and IPL annealing steps were carried out in the ambient with relative humidity of 60%. Right after perovskite annealing, the substrates were transferred to a nitrogen filled glovebox for the Spiro-MeOTAD hole-transport layer deposition. The Spiro-MeOTAD solution was made by dissolving 72.3 mg of Spiro-MeOTAD in 1 mL chlorobenzene, pipetting 28.8 µL 4-tert-butyl-pyridine, 17.5 µL of a stock solution of 520 mg/ml lithium bis (trifluoromethylsulphonyl) imide in anhydrous acetonitrile, and 29 µL of the cobalt dopant FK209 TFSI salt (300 mg/ml in anhydrous acetonitrile) to the mixture to prepare the final solution. The Spiro-MeOTAD film was made by spin-coating 70 µL of the prepared solution at 1700 rpm for 30 seconds to achieve 200 nm thickness. Finally, 80 nm gold electrode was deposited through a thermal evaporator.

3. RESULTS AND DISCUSSION

Herein, we investigated the impact of IPL on rapid post processing of the ETL and absorber thin films for n-i-p structure PSCs with glass/FTO/TiO_2/$CH_3NH_3PbI_3$/Spiro-MeOTAD/gold as well as glass/FTO/SnO_2/$Cs_{0.05}(MA_{0.85}FA_{0.15})_{0.95}PbI_3$ /Spiro-MeOTAD/gold architecture. In the first architecture, we only studied the synergy of IPL and CH_2I_2 on device efficiency, while in the latter form, we added CH_2I_2 to the mixed triple cation formulation and applied IPL to sinter both SnO_2 and perovskite photoactive films. Each thin film fabrication includes a coating process followed by rapid thermal annealing. The resulted thin films should possess high crystallinity, high uniformity and free of morphological defects such as pinholes or cracks to achieve optimum efficiency. To achieve these goals various techniques such as antisolvents, use of additives, application of special inert environments, sequential coating and annealing steps have been applied. In this interim, we have fabricated PSCs through RTA using IPL with respect to the application of these realms, particularly the use of additives which can aid cheap and rapid fabrication of efficient PSCs in the ambient.

3.1 IPL on Perovskites

Crystallization and film morphology are pivotal factors to obtain PSCs with high efficiency and stability. This process includes two sub-steps of nucleation and grain growth starting from the deposition process and lasting till the end of post process annealing. The perovskite film is typically fabricated using the potential coating techniques such as spin-coating for lab scale research and development, and slot-die coating for large scale industrial manufacturing. Therefore, understanding and providing the optimal crystallization plays a significant factor on device performance. The perovskite coating starts from spinning the precursor solution with the addition of a small quantity of a poor solvent, such as chlorobenzene, during the last few seconds of the spinning process. At this stage, the supersaturation takes place and the perovskite molecules and atoms cluster and form high density nucleation steps which then grow upon annealing. Perovskite films with poor supersaturation have sparse molecules of the solution which then provides low nucleation density states, thus providing poor perovskite film morphology and device performance. Despite significance of the appropriate selection of antisolvent with respect to the precursor solvent and concentration, nucleation pace of the supersaturated solution plays a significant role on providing the ultra-smooth and superior films. Nucleation and growth dynamics determine the series and shunt resistance pathways which, in turn, affect the charge extraction and transportation throughout the films and, thus, device efficiency. The nucleation pace upon coating and annealing can be controlled through the application of additives. In this interim, alkyl halides have been introduced as potential candidates to performs this task. Chueh et. al [10] investigated the role of various alkyl halide additives to investigate their device performance.

Di-iodomethane (CH_2I_2) is a potential alkyl halide with good solubility in perovskite polar solvents and has a higher boiling point than the perovskite precursor average boiling point, thus, addition of this alkyl halide to the perovskite precursor was found to boost the PSCs efficiency [11]. To fabricate our PSCs, we heated the perovskite wet films for 30 seconds on a hotplate to evaporate the solvents and transferred the slides immediately to the IPL machine for rapid sintering and crystal growth. Fig. 1 shows the top surface SEM images of the CH_2I_2 added perovskite films before and after IPL annealing on the $CH_3NH_3PbI_3$ perovskite films. As shown in Fig. 1(A), the perovskite films without CH_2I_2 additive delineated discontinuities with smaller grains after IPL annealing, while the films with CH_2I_2 additive (Fig. 1(B)) indicated continuous films without any pinholes or cracks. These observations imply two significant roles of the IPL-CH_2I_2 synergy. First, the energetic flashes of light, particularly the UV portion, could cleave the C-I bonds of the CH_2I_2 additive, thus releasing iodine which could act as a binder to stitch the grains and avoid the formation pinholes. Second, the CH_2I_2 could retard the crystallization due to its high boiling point, thus, increasing the crystal growth after IPL annealing.

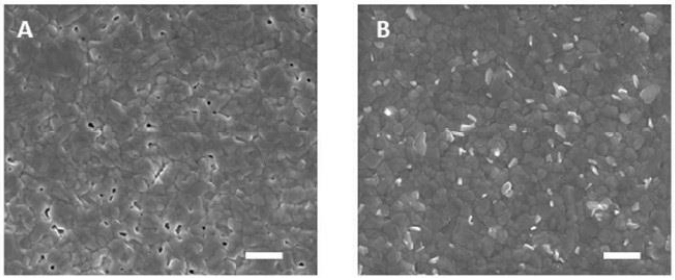

FIGURE 1: TOP SURFACE SEM IMAGE OF THE IPL ANNEALED PEROVSKITE FILMS A) WITHOUT, AND B) WITH CH_2I_2 ADDITIVE (SCALE BAR = 1 MICRON) [11].

To determine the phase purity upon RTA through IPL, we obtained the XRD patterns of the perovskite films as shown in Fig. 2. The intense 2θ peaks around 14.1° and 28.4° indicates highly crystalline perovskite grains with tetragonal structure grown favorable to (110) and (220) planes. The intense 2θ peaks around 26.5°, 33.75°, 37.5°, 51.2°, and 54.5° are indicative of FTO/SnO_2, and the other strong peaks around 20°, 24.4°, 31.8°, 34.9°, 40.5°, 43°, and 50.5° are associated to (112), (202), (310), (312), (224), (314), and (404) crystal planes of perovskite tetragonal black phase. Surprisingly, the XRD patterns did not reveal any PbI_2 phase at 12.4° which indicates that the annealing processes were adequate and enough to convert the yellow phase to the pure perovskite black phase capable of producing charge carriers. It is noteworthy that both films did not reveal any degradation phase, however, the peak intensity for almost all perovskite planes fabricated from CH_2I_2 added precursor were higher which indicates higher crystallinity and is consistent with the observed larger grains within the SEM images. Fig. 3 also shows the higher UV-Vis absorption for the perovskite films made from the alkyl halide additive. The enhanced absorption can be attributed to the disappearance of pinholes and less grain boundary density as the result of increased grain sizes and complies with the morphology enhancement observed through SEM.

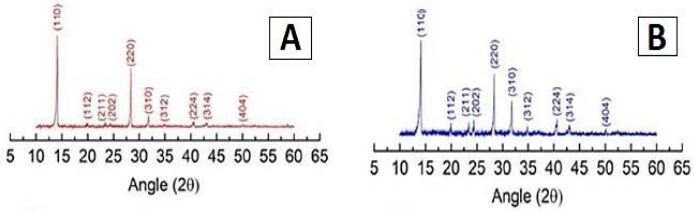

FIGURE 2: XRD PATTERNS OF THE IPL ANNEALED PEROVSKITE FILMS A) WITHOUT, AND B) WITH CH_2I_2 ADDITIVE [11].

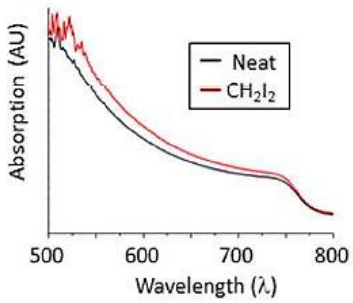

FIGURE 3: UV-VIS ABSORPTION SPECTRA OF THE IPL ANNEALED PEROVSKITE FILMS [11].

To measure the device functionality, voltammetry measurement was carried out using an AM 1.5 simulated light from a Newport LCS-100 solar simulator, in which, each cell was illuminated from the back side with an active area of 0.12 cm^2. Fig. 4 shows the J-V curves, demonstrating the forward and reverse scans of the champion cells for the PSCs with and without CH_2I_2 additive after IPL annealing, exhibiting 16.5% and 10% efficiency, respectively. The results pertinent to 5 PSCs without CH_2I_2 additive demonstrated the average V_{OC}, J_{SC}, fill factor (FF), and efficiency of 0.84 V, 21.7 mA/cm^2, 44.4%, and 8% for, respectively; whereas the results for 10 PSCs made from the CH_2I_2 assisted precursor was found to considerably enhance these photovoltaic parameters to 0.99 V, 23.7 mA/cm^2, 65.1%, and 15.3%, respectively. Interestingly, the CH_2I_2 perovskite films annealed through IPL with blocked UV portion demonstrated poor device performance with hysteresis which indicated that the UV portion was pivotal for CH_2I_2 dissociation and boosting the annealed perovskite film morphology.

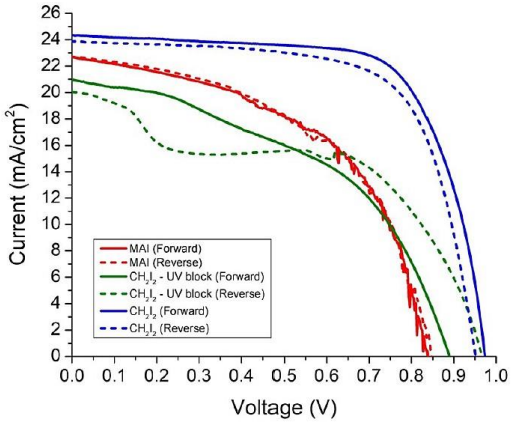

FIGURE 4: J-V CURVES FOR THE PSC WITH AND WITHOUT CH_2I_2 ADDITIVE [11].

3.2 IPL on SnO_2

We previously investigated the simultaneous impact of IPL on the grain growth with in-situ stitching of the grain boundaries through cleavage of chemical bonds within the CH_2I_2 alkyl halide. In another work, we applied IPL on the mixed triple cation perovskite formulation with CH_2I_2 additive to investigate the IPL- CH_2I_2 within a new perovskite chemistry and to also rapidly crystallize and sinter the potential inorganic metal oxides such as SnO_2 [12]. TiO_2 and SnO_2 are the two potential ETL materials used in fabricating perovskite solar cells. TiO_2 should be processed using high temperature furnaces as high as 500°C which is not favorable for high throughput and economical fabrication of PSCs and is not compatible with roll to roll favorable plastic substrates. However, SnO_2 has a higher electron mobility, better band alignment to the perovskite absorber, and requires less temperature for crystallization. Therefore, direct annealing of the potential PSC charge carrier layers through IPL provides rapid and economical fabrication of PSCs, thus, decreasing the energy payback time of the fabricated modules through eliminating prolonged high temperature annealing. In the first step, we applied IPL to directly anneal the SnO_2 ETL formed upon spin coating of a diluted solution of the SnO_2 colloidal dispersion on FTO. Upon spinning, most of the water content evaporated and the remained SnO_2 was transferred to the IPL machine for sintering using two different energy densities of 1.4 kJ, and 2.1 kJ, with different pulse counts of 1, 5, 10, and 15, each lasting for 2 ms followed by one second delay between pulses. Due to the SnO_2 films being extremely thin, we could not observe any peaks through XRD, thus, we investigated the chemical state through XPS. Fig. 5(A) shows the XPS spectrum indicating the Sn and O1S state peaks of the SnO_2 films annealed through various IPL conditions. As it is apparent, the binding energy associated with the 2.1 kJ – 5 pulse condition was the highest indicating 531.25 eV, which can indicate that the Sn-O bonding was strengthened, thus charge transportation could be facilitated at this condition. Similarly, the obtained binding energy for Sn^{4+} of the $Sn3d_{3/2}$, and $Sn3d_{5/2}$ state (Fig. 5(B)) was higher compared to other condition, indicating 486.7 eV and 495.15 eV, respectively. The synergy of these states suggests enhanced sintering and crystallization of the SnO_2 film, thus, enhanced charge transportation.

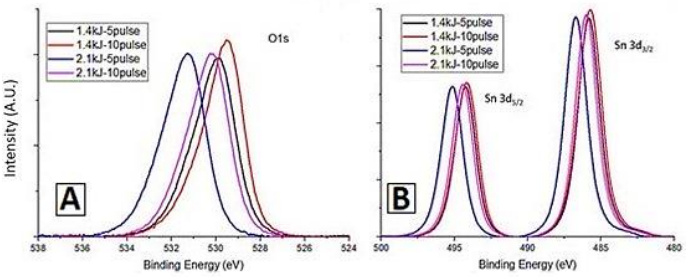

FIGURE 5: A) O1S STATE, AND B) Sn PEAKS OF THE SnO_2 FILMS ANNEALED THROUGH VARIOUS IPL CONDITIONS [12].

To further study the applicability of IPL-CH_2I_2 synergy in another perovskite chemistry, CH_2I_2 was added to the mixed cation $Cs_{0.05}(MA_{0.85}FA_{0.15})_{0.95}PbI_3$ perovskite ink and annealed through IPL using 5 pulse counts, each with 2 ms duration and

1.4 kJ energy. As shown in Fig. 6, the top surface SEM images indicated 1.45 times larger grains with diminished dendrite structures formed in the absence of the alkyl halide. This indicate that the neat mixed cation precursor could undergo natural annealing during the spinning process, thus conducting inadequate crystallization. To examine annealing adequacy, we obtained the XRD patterns of the perovskite film after IPL annealing. As apparent in Fig. 7, the intense peaks of the (110) and (220) perovskite peaks with no signs of the unconverted or degraded PbI_2 phase was observed which can imply sufficient and adequate thermal annealing.

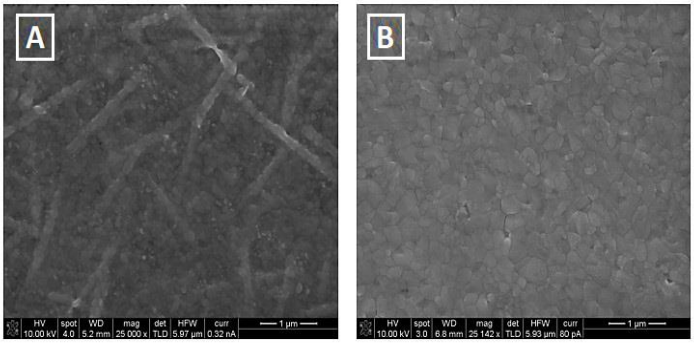

FIGURE 6: TOP SURFACE SEM IMAGE OF THE IPL ANNEALED MIXED TRIPLE CATION PEROVSKITE FILMS A) WITHOUT, AND B) WITH CH_2I_2 ADDITIVE [12].

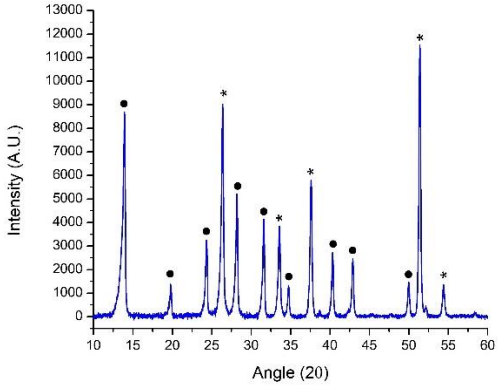

FIGURE 7: XRD PATTERN OF THE IPL ANNEALED PEROVSKITE (• PEAKS) ON SnO_2 (* PEAKS) ANNEALED THROUGH OPTIMAL IPL CONDITION [12].

Fig. 8 shows the photovoltaic parameters of IPL annealed perovskite and SnO_2 thin films. As shown, devices with SnO_2 films annealed through 5 pulse counts each carrying 2.1 kJ energy indicated the highest performance, illustrating V_{OC}, J_{SC}, fill factor (FF), and efficiency of 1.02 V, 15.78 mA/cm^2, 78.3%, and 12.56%, and the average of 0.995 V, 15.85 mA/cm^2, 76.3%, and 11.98% for 5 devices, respectively. The other IPL annealing conditions resulted in lower photovoltaic efficiency, resulting in the average efficiency of 6.78%, 9.27%, and 9.56% for the 1.4 kJ – 5 Pulse, 1.4 kJ – 10 Pulse, and 2.1 kJ – 10 Pulse conditions for 5 devices in each condition. It is noteworthy that for the pulse counts more than 5, the current density was lowered and remained constant for 15 pulses, while pulse counts less than 5 resulted in dead cells with resistor behavior within the J-V curves. This indicates that the pulse count, in parallel to the heat flux per flash, play a significant role on device performance. Up to our knowledge this was the first reported work and the fastest rout of processing PSCs which is also directly applicable for roll to roll manufacturing of PSCs.

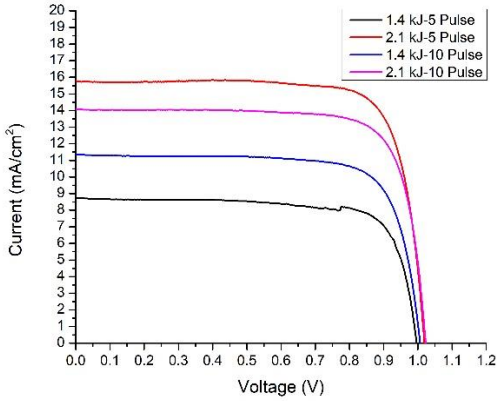

FIGURE 8: J-V CURVES OF THE PSCs FABRICATED THROUGH DIFFERENT IPL ANNEALING CONDITIONS ON SnO_2 FILMS [12].

4. CONCLUSION

We showed that the IPL-CH_2I_2 synergy is applicable for different perovskite chemistries and could enhance the photovoltaic parameters of PSCs by supplying the films with cleaved iodine by the UV portion of the IPL and retarding the crystallization as the result of enhanced solution boiling point. Also, rapid fabrication of PSCs through direct IPL annealing was introduced, in which, IPL was applied on both SnO_2 electron transport layer and perovskite films and can be directly used for automated manufacturing of PSCs through roll to roll.

ACKNOWLEDGEMENT

The authors are thankful to the Conn center for renewable energy research for providing financial support and research facilities.

REFERENCES

[1] https://www.nrel.gov/pv/cell-efficiency.html.
[2] Dong, Q.; Fang, Y.; Shao, Y.; Mulligan, P.; Qiu, J.; Cao, L.; Huang, J., Science 2015, 347 (6225), 967-970.
[3] Filip, M. R.; Eperon, G. E.; Snaith, H. J.; Giustino, F., Nature communications 2014, 5, 5757.

[4] Hao, F.; Stoumpos, C. C.; Cao, D. H.; Chang, R. P. H.; Kanatzidis, M. G., Nature Photonics 2014, 8 (6), 489-494.
[5] Yang, Z.; Surrente, A.; Galkowski, K.; Bruyant, N.; Maude, D. K.; Haghighirad, A. A.; Snaith, H. J.; Plochocka, P.; Nicholas, R. J., The journal of physical chemistry letters 2017, 8 (8), 1851-1855.
[6] Wu, Q.; Zhou, P.; Zhou, W.; Wei, X.; Chen, T.; Yang, S., ACS applied materials & interfaces 2016, 8 (24), 15333-15340.
[7] Ko, H.-S.; Lee, J.-W.; Park, N.-G., Journal of Materials Chemistry A 2015, 3 (16), 8808-8815.
[8] Jung, J. W.; Williams, S. T.; Jen, A. K. Y., RSC Advances 2014, 4 (108), 62971-62977.
[9] Ghahremani, A. H.; Martin, B.; Ankireddy, K.; Druffel, T., *Journal of Coatings Technology and Research* 2019, *16* (6), 1637-1642.
[10] Chueh, C.-C.; Liao, C.-Y.; Zuo, F.; Williams, S. T.; Liang, P.-W.; Jen, A. K.-Y., Journal of Materials Chemistry A 2015, 3 (17), 9058-9062.
[11] Ankireddy, K.; Ghahremani, A. H.; Martin, B.; Gupta, G.; Druffel, T., Journal of Materials Chemistry A 2018, 6 (20), 9378-9383.
[12] Ghahremani, A. H.; Martin, B.; Gupta, A.; Bahadur, J.; Ankireddy, K.; Druffel, T., Materials & Design 2020, 185, 108237.